

The Magellanic Cloud Calibration of the Galactic Planetary Nebula Distance Scale

Letizia Stanghellini

National Optical Astronomy Observatory, 950 N. Cherry Av., Tucson, AZ 85719
 lstanghellini@noao.edu

Richard A. Shaw

National Optical Astronomy Observatory, 950 N. Cherry Av., Tucson, AZ 85719
 shaw@noao.edu

Eva Villaver¹

Space Telescope Science Institute, 3800 San Martin Drive, Baltimore, MD 21218
 villaver@stsci.edu

ABSTRACT

Galactic planetary nebula (PN) distances are derived, except in a small number of cases, through the calibration of statistical properties of PNe. Such calibrations are limited by the accuracy of individual PN distances which are obtained with several non-homogeneous methods, each carrying its own set of liabilities. In this paper we use the physical properties of the PNe in the Magellanic Clouds, and their accurately known distances, to recalibrate the Shklovsky/Daub distance technique. Our new calibration is very similar (within 1%) of the commonly used distance scale by Cahn et al. (1992), although there are important differences. We find that neither distance scale works well for PNe with classic ("butterfly") bipolar morphology, and while the radiation bounded PN sequences in both the Galactic and the Magellanic Cloud calibration have similar slopes, the transition from optically thick to optically thin appears to occur at higher surface brightness and smaller size than that adopted by Cahn et al. The dispersion in the determination of the scale factor suggests that PN distances derived by this method are uncertain by at least 30%, and that this dispersion cannot be reduced significantly by using better calibrators. We present a catalog of Galactic PN distances using our re-calibration which can be used for future applications, and compare the best individual Galactic PN distances to our new and several other distance scales, both in the literature and newly recalibrated by us, finding that our scale is the most reliable to date.

Subject headings: Planetary nebulae: general; distances

1. Introduction

The uncertainty associated with distances measurements of Galactic planetary nebulae (PNe) is a major obstacle to the advancement of PN research.

Only ~ 40 Galactic PNe have distances that have been determined individually with reasonable accuracy. Distances to Galactic PNe can be determined individually in various ways, including cluster membership (Chen et al. 2003, CHW03; Alves et al. 2000, ABL00), by measuring the rate of their expansion (e. g., Liller & Liller 1968, LL68; Hajian

¹Affiliated with the Hubble Space Telescope Division of the European Space Agency

et al. 1995, HTB95), by the reddening method (e. g., Gathier et al. 1986, GPP96; Kaler & Lutz 1985, KL85), and by measuring their spectroscopic parallax (Ciardullo et al. 1999, C99) or trigonometric parallax (Harris et al. 2007, Hea07).

For the remaining >1800 Galactic PNe (Acker et al. 1992) one has to rely on statistical distance scales, whose calibrations are based on the reliability of the individually known PN distances, and the validity of a general correlation that links the distance-dependent to the distance-independent physical properties of PNe. The Cahn, Kaler, & Stanghellini (1992, CKS) distance scale of Galactic PNe is based on an attempt by Daub (1982, D82) to improve Shklovsky’s distance scale (Shklovsky 1956a, 1956b) for optically thick nebulae. Shklovsky’s distance scale assumes that all PNe have equal (observed) ionized mass. D82 assumed that Shklovsky’s constant mass approach was still valid, but only for those PNe that are optically thin to the Lyman continuum radiation emitted by the central stars (density bounded). For the optically thick (radiation bounded) PNe, D82 based the distance scale on a calibration of an ionized mass versus surface brightness relation. CKS improved D82’s calibration with the use of a larger number of calibrators (PNe with known individual distance), and calculated the statistical distances to 778 Galactic PNe.

Since its publication, distances from the CKS catalog have been used preferentially and widely in the literature. Other statistical methods that have been commonly used include those by Maciel (1984), Zhang (1995, Z95), van de Steene & Zijlstra (1995, vdSZ), Schneider & Buckley (1996, SB96) and Bensby & Lundström (2001, BL01). All these distance scales rely on a set of Galactic calibrators whose distances are mostly derived from reddening or expansion properties, or from the assumption of Galactic Bulge membership, with all the consequent uncertainties. With the publication over the past decade of critical physical parameters for a large sample of Magellanic Cloud PNe (Shaw et al. 2001, 2006; Stanghellini et al. 2002, 2003), including highly accurate $H\beta$ fluxes, physical dimensions, morphologies, and extinction constants, we have the opportunity to assess and improve the distance scale for Galactic PNe. In this paper we take advantage of the wealth of Magellanic Cloud PN

data to re-calibrate the CKS distance scale, as well as other distance scales for comparison. Homogeneously determined photometric radii from *HST* of a PN sample with low Galactic reddening are the best way to determine any relation that involves apparent diameters. Furthermore, the relatively recent publication of trigonometric and spectroscopic parallax and cluster membership distances to Galactic PNe allow us to test with unprecedented reliability our own and other distance scales.

The construction of any statistical distance scale for PNe is composed of three fundamental steps: the selection of a *method* that has some physical or empirical basis, the selection of a set of *calibrator PNe*, for which distances have been determined by some independent means, and an analysis of the *applicability* of the calibration to a wide variety of PNe. Until now it has been difficult to compare the viability various methods, since their calibrations and applications have varied so widely. In §2 we describe in detail the Shklovsky/Daub/CKS distance scale and the superiority of the Magellanic Cloud PNe as calibrators. We also derive our new calibration of this method and assess its inherent uncertainties. In §3 we discuss the physical underpinning of the CKS distance method in light of recent advances in modeling the evolution of PNe. In §4 we take a closer look at the viability of various methods for determining independent distances to Galactic PNe (i.e., the set that had previously been used as calibrators), and discuss the applicability of the Magellanic Cloud distance scale to Galactic PNe. In §5 we recalibrate the most used statistical distance methods with the Magellanic Cloud PNe, and then compare the accuracy of these methods to one another using the best independently determined distances to Galactic PNe. We conclude in §6 with our final prescription and recommendation for determining statistical distances to Galactic PNe.

2. The Magellanic Cloud Calibration and the New PN Distance Catalog

The CKS statistical distance scale is based on the calibration of the relation between D82’s *ionized mass*

$$\mu = (2.266 \times 10^{-21} D^5 \theta^3 F)^{1/2} \quad (1)$$

and the *optical thickness parameter*

$$\tau = \log \frac{4\theta^2}{F}, \quad (2)$$

where D is the distance to the PN in parsecs, θ is the nebular radius in arcsec, and F is the nebular flux at 5 GHz. The parameter μ increases as the ionization front expands into the nebula. Once a PN becomes density bounded, μ remains constant for the rest of the observable PN lifetime.

By calculating μ and τ for several PNe with known distances, dimensions, and fluxes, CKS derived the μ - τ relation:

$$\log \mu = \tau - 4, \quad \tau < 3.13 \quad (3a)$$

$$\log \mu = -0.87, \quad \tau > 3.13, \quad (3b)$$

where Eq. 3a holds for PNe of high surface brightness, and Eq. 3b for PNe with low surface brightness.

The calibration of the above distance scale was based upon 19 Galactic PNe with independent distances with comparatively poor accuracy. At the time when the CKS paper was written there were hardly any Magellanic Cloud PNe with accurately measured diameters, and the distances to the Magellanic Clouds were also quite uncertain. We can now re-calibrate the distance scale using the nebular parameters relative to the LMC and SMC PNe observed by us with the *Hubble Space Telescope (HST)* (Shaw et al. 2001, 2006; Stanghellini et al. 2002, 2003). In order to determine τ and μ for Magellanic Cloud PNe we use a transformation between the 5 GHz and the H β fluxes (Eq. 6 in CKS), since radio fluxes are not available for Magellanic Cloud PNe. All other parameters are available in our *HST* paper series. Note that we use the photometric radius as the proper measure of the nebular dimension, which is defined as the radius that includes 85% of the flux in a monochromatic emission line.

We have adopted a distance to the LMC of 50.6 kpc (Freedman et al. 2001; Mould et al. 2000), which is accurate to $\sim 10\%$ (Benedict et al. 2002). The variation in the adopted distance when applied to individual objects can be easily estimated given that the three dimensional structure of the

LMC has been well established (Freeman, Illingworth, & Oemler 1983; van der Marel & Cioni 2001). The LMC can be considered a flattened disk with a tilt of the LMC plane to the plane of the sky of 34° (van der Marel & Cioni 2001). Freeman, Illingworth, & Oemler (1983) derived a scale height of 500 pc for an old disk population. The scale height of young objects is between 100 to 300 pc (Feast 1989). Using the scale height of an old disk population the 3D structure of the LMC introduces a variation in the adopted distance smaller than 1% from object to object and therefore has been neglected in the calibration.

For the SMC we have used a distance of 58.3 kpc (Westerlund 1997). The accuracy of this distance is not as well established as for the LMC. Moreover, the SMC is irregular with a large intrinsic line of sight depth (between 6 and 12 kpc: Crowl et al. 2001) which varies with the location within the galaxy. We have estimated an average line of sight depth of 5 kpc for the PNe in our sample by combining the span of the positions (400 pc in right ascension and 2 kpc in declination) of the PNe with respect to the optical center of the SMC with the dispersion in the distance to the SMC derived by Crowl et al. (2001) using SMC clusters positions. The distance uncertainty introduced by this depth in the SMC is roughly 9%, still low to significantly affect the result but one order of magnitude larger than the one obtained for the LMC. In this respect we consider LMC PNe to be better calibrators than the SMC PN for the distance scale.

In Figure 1 we show the LMC PNe on the $\log \mu$ - τ plane. We have calculated τ and $\log \mu$ as explained above, and assumed $D_{\text{LMC}}=50.6$ kpc. In the Figure we plot the different morphological types with different symbols, following the classification in Shaw et al. (2001, 2006). To guide the eye we have plotted, on the figure, the Galactic distance scale fit from CKS (solid line). The optically thick sequence of LMC PNe is very tight for $\tau < 2.1$, and most LMC PNe are optically thin for $\tau > 2.1$. The fitted value of the function for optically thin LMC PNe is almost identical to that of Galactic PNe *if we exclude bipolar planetary nebulae*. The broken line in Figure 1 corresponds to the Magellanic Cloud fit of the optically thick sequence of LMC PNe (see Eq. 4a and 4b below). Similarly, in Figure 2 we show the same plot

of Figure 1, but for SMC PNe. The morphology and sizes of the nebulae are from Stanghellini et al. (2003). Even with the scarcity of data points, the thick PN sequence is well defined by SMC PNe, and it is identical to that of the LMC PNe.

The observed ionized masses of bipolar PNe in both Figures 1 and 2 appear mostly well above the constant ionized mass line. The parameters μ and τ have been calculated with the photometric radii of the PNe, that can be very different from the isophotal radii in the case of PNe with large lobes. Furthermore, bipolar PNe might be optically thick for most of their observed lifetime (Villaver et al. 2002a), and thus are not the ideal calibrators for the optically thin PNe branch of the $\log \mu - \tau$ relation. In deriving the distance scale based on Magellanic Cloud PNe we thus exclude PNe with bipolar morphology. This leave us with 70 Magellanic Cloud calibrators, a very large number of PNe with individual distances when compared to the 19 calibrators in CKS. In Figure 3 we show the Magellanic Cloud calibration of the PN distance scale, where open symbols are LMC PNe and filled symbols are SMC PNe, and where we exclude bipolar PNe. Note that we have assumed that the ionized mass for optically thin PNe is constant, as in D82 and CKS.

The fit to the distance scale based on the Magellanic Cloud PNe (this paper, hereafter SSV) is:

$$\log \mu = 1.21 \tau - 3.39, \tau < 2.1 \quad (4a)$$

$$\log \mu = -0.86, \tau > 2.1 \quad (4b)$$

The solid line in Figure 3 shows this relation. The separation between optically thick and thin PNe is very obvious from the figure, and the optically thick sequence is much better defined here than in CKS, thanks to the use of the best calibrators available now. The optically thick sequence has been derived by least-square fit, and has correlation coefficient $R_{xy}=0.8$. The optically thin sequence is determined by the average of the $\log \mu$ for $\tau > 2.1$. Using another estimate of the central tendency will change the horizontal scale by less than 5%, which is well within the uncertainty. Furthermore, if we were to fit the data points of Figure 3 with just one line for all τ we would have a very poor correlation ($R_{xy}=0.14$), which reinforce the evolutionary scheme of optically thick to

thin PNe, proposed by D82 to improve Shklovsky's method.

By examining Figure 3 we infer that: (1) Our analysis allows us to confirm the CKS distance scale for optically thin PNe; (2) the optically thick sequence is very well defined by the Magellanic Cloud PNe and it is different from that of CKS; (3) the new statistical distance for optically thin PNe increases slightly the assumed ionized mass, such that distances for optically thin nebulae are typically 1% larger compared to those computed using the CKS calibration. (4) bipolar PNe do not follow the empirical relation, and their ionized mass actually increases steadily with τ , confirming that they stay in the ionization bound state for much longer than PNe with other morphological types. The probable reason why the bipolar PN relation does not flatten out for $\tau > 2.1$ is because they are the progeny of the more massive stars and they are expected to remain optically thick (given a combination of the large circumstellar densities and fast evolution of the central star).

By using the SSV distance scale we calculated the statistical distances to all non-bipolar PNe in the LMC and the SMC. We obtain distributions that are nicely narrow, with mean values (and dispersions), $D_{LMC}=50.0\pm 7.5$ kpc and $D_{SMC}=57.5\pm 5.5$ kpc, that are within 1% of the distances to the Magellanic Clouds.

We applied our new distance scale to the large sample of Galactic PNe in the original CKS catalog, and present the revised distances in Table 1. Column (1) gives the usual name as in CKS, column (2) gives the calculated τ , columns (3) and (4) give the angular radius and the flux used in the calculation, and column (5) gives the distance to the PNe. Note that the fluxes in (4) are the 5 GHz fluxes from CKS when available, or their H β equivalents.

3. The Physics of the Statistical Distance Scale

As CKS pointed out, the assumption of constant ionized mass for optically thin PNe (or that it can be computed for optically thick PNe with a one-parameter model) would seem to be a doubtful proposition since the progenitor stars vary in mass by nearly an order of magnitude. CKS minimized the significance of the variation in ionized

mass by pointing out that distances so derived depend only on the square-root of the assumed mass. One might also expect that the ionized mass would be fairly directly correlated with the progenitor mass. However, hydrodynamical models of the co-evolving PN and central star by Villaver et al. (2002a) show that the decline of gas density with radius is generally quite steep (except within the bright inner shell of gas) over a wide range of progenitor masses and during the entire visible lifetime of the nebula. The implication is that, for optically thin nebulae, the bulk of the mass exists in the faint, low-density, outer halo. Since the volume emissivity of recombination lines is proportional to the square of the gas density, the massive nebular halo contributes very little to the observed emission. Most published values for PN masses assume a constant density for the gas, one that is only representative of the bright inner shell, leaving the bulk of the PN mass unaccounted for. In part for these reasons, ionized masses derived in this way reflect only a modest fraction of the total mass of the nebula, such that the assumption of a constant mass is sufficiently accurate to render the Shklovsky distance method useful.

We have shown that the distance method of CKS is empirically sound, and derived the scale factor for optically thin PNe to that from observations of Magellanic Cloud PNe. It is important to note the significance of the *dispersion* in the PN masses (expressed in the μ parameter) about the mean in the calibration shown in Figure 3. The $1 - \sigma$ deviation about the mean value is 0.28, which translates to a corresponding uncertainty in the distance of about 30%. We regard this value as a rough estimate of the minimum uncertainty that may be associated with the distance to an individual PN derived using this methodology. It is important to note that the uncertainty in the distance scale *cannot* be reduced with improved calibrator nebulae, since the distance uncertainty is of order 10% (i.e., of order the size of the symbols in Figure 3). The scatter in the data results from genuine variations in the ionized masses of the calibrator nebulae, and quantifies the fundamental limitation in this technique.

The new PN distance scale (SSV) is very similar to that of CKS, with the exception of the transition between optically thick and optically thin stages. From Eq. 4b, the definition of μ , and the

relation $D = 206265 R_{\text{PN}}/\theta$ (where R_{PN} is the linear nebular radius in pc) we can determine the radius at which the PN becomes optically thin. For $\tau = 2.1$ we obtain $R_{\text{PN}} \sim 0.06$ pc. The same calculation to determine the PN radius at which the thick to thin transition occurs by using Eq. 3b and $\tau = 3.13$ gives $R_{\text{PN}} \sim 0.09$ pc. The uncertainty in the determination of τ at transition, and thus of R_{PN} , depends on the scatter of the ionized mass calibrators used in CKS. The new calibration is much more reliable.

The metallicities of the LMC and SMC are, on average, of the order of half and a quarter that of the solar mix respectively (Russell & Bessell 1989; Russell & Dopita 1990). The AGB wind is likely to be dust driven, therefore it has a strong dependency on metallicity. It is then expected that LMC and SMC stars with dust-driven winds lose smaller amounts of matter (Winters et al. 2000) during the AGB phase than their Galactic counterparts. The mass-loss history during the AGB determines the circumstellar density structure that will eventually constitute the PN shell (Villaver et al. 2002b). A reduced mass-loss rate during the AGB has the effect of decreasing the density of the circumstellar envelope prior of PN formation.

Furthermore, after the envelope is ejected, the remnant central star leaves the AGB and its effective temperature increases. The stellar remnant becomes a strong emitter of ionizing photons, responsible for ionizing the nebula. The mechanism that drives the wind during the central star phase (with velocities a few orders of magnitude higher than that experienced during the AGB phase) is the transfer of photon momentum to the gas through absorption by strong resonance lines (Pauldrach et al. 1988). The efficiency of this mechanism depends on metallicity, thus it is expected to be less efficient in Magellanic Cloud central stars than in the Galactic ones, with correspondingly lower escape velocities for the winds, and a decreased efficiency in shell snow-plow.

As has been shown by Villaver et al. (2002a), the propagation of the ionization front determines the density structure of the nebula early in its evolution, while the pressure provided by the hot bubble has no effect at this stage. The propagation velocity of the Strömgren radius, which ultimately determines the transition from the optically thick to the optically thin stages, depends mainly on

the ionizing flux from the star and on the density of the neutral gas. Given the dependency of the AGB mass-loss rates on metallicity, the ionization front will encounter a lower neutral density structure in Magellanic Cloud PNe than in Galactic PNe. This would tend to make the transition from optically thick to thin at a smaller radius in Magellanic Cloud PNe than in Galactic PNe. The fact that our Magellanic Cloud calibration of the CKS scale occurs at smaller radii than that derived by CKS is probably coincidence. On the other hand, if we really could determine empirically the transition radius as a function of metallicity, we would expect two different thick sequences for the SMC and the LMC PNe, given their different metallicity, and yet the sequences are almost identical (Figs. 1 and 2). That is, we do not see the effects of metallicity on our distance scale, and that is applicable to Galactic PNe as well. We discuss below (§4) how the newly derived distances match extremely well with the best individual distances to Galactic PNe independently of metallicity.

4. Comparison of our Distance Scale to Individual Galactic PN Distances

We have assessed that our new calibration of the PN distance scale is very similar to that of CKS, but with a revision in the transition between the radiation bounded and the density bounded stages. The comparison between the CKS and the SSV scales suffers from the fact that part of the CKS calibrators are obsolete, and that new Galactic calibrators have become available. It is worthwhile to compare the SSV scale with the best available individual distances to Galactic PNe to date before we confirm the validity of the new calibration.

In Table 2 we give the best set of individual Galactic PN distances available to date. Column (1) gives the common name; columns (2) and (3) give the best individual distance and, where available, its uncertainty; columns (4) and (5) give respectively the statistical distances for the same PNe from CKS and the SSV; columns (6) and (7) give the distance determination method (CM for cluster membership, P for parallax, E for expansion, R for reddening, see explanations below) and its reference. We have selected a sample of individual Galactic PN distances based on the lit-

erature, and whose statistical distances have been calculated by CKS and can be derived for the SSV calibration as well.

The best methods to get individual PN distances are (1) trigonometric parallax, (2) the use of a spectroscopic companion of the PN central star, which allows to derive the spectroscopic parallax, and (3) the membership of the PN in an open or globular cluster. Apart from trigonometric parallaxes, that are applicable only for nearby PNe, the distance to the PN is that of a companion or a cluster, whose uncertainties are typically much lower than those related to other methods for PN distances. In the past decade there have been two major studies of PN parallaxes. C99 used *HST* imaging to determine central star companions of a PN sample, obtaining ten probable associations and the relative spectroscopic parallaxes. We list all of these in Table 2, except for A 31, where only a lower limit to the distance is given, and A 33 and K 1-27, whose distances seem to be controversial in C99. Hea07 published trigonometric parallaxes of several Galactic PNe. Following the discussion in Hea07, we include all their final determinations in Table 2, including the uncertainties. Planetary nebulae whose distances have been derived through cluster membership are the PN in Ps 1, whose distances has been recalculated by ABL00, and that in the open cluster NGC 2818, whose distance has been estimated by CHW03. It is worth noting that Mermilliod et al. (2001) found that the radial velocity of the NGC 2818 PN is slightly lower than that of the cluster, making its membership marginally questionable.

Since CKS was published there have been other PNe observed in clusters, including JaFu1 and JaFu2 (Jacoby et al. 1997), and a PN in M 22 (Monaco et al. 2004), but their distances are not included in Table 2 either because their cluster membership is not definitive or because their nature is still uncertain, as described in detail in the discovery papers.

An alternative method for PN distances is the determination of the secular PN expansion, a method that had its renaissance with the use of the accurate relative astrometry afforded by the *HST*. In this category we found distances to several PNe by Hajian et al. (1993, 1995, 1996; HBT93, HBT95, HT96), Palen et al. (2002,

Pea02), Gomez et al. (1993, GRM93), and also the work by LL68. Among the distances determined by expansion we have only listed in Table 2 those deemed reliable by the authors listed above. In particular, in Pea02 there are several distances determined by different expansion algorithms, and if the results are very different by different methods for the same PN we have excluded them. Uncertainties in expansion distances, when available, are much higher than those of parallaxes or cluster membership, and the method is intrinsically less reliable, given the impossibility of following the PN acceleration history, and the modeling difficulty given unknown process as such as differential mass-loss.

Finally, a very rough individual distance can be derived in some cases by studying the reddening patches around the PN and then building reddening-distance plots for the known stars surrounding the PN. This method, although providing several data-points in the literature, is the most uncertain given the inhomogeneity of the Galactic ISM. GPP96 derived reddening distances for several PNe, and we used in Table 2 only the reliable ones, as deemed by the authors. We have excluded NGC 2346, since the scatter in its distance-reddening plot is overly large. KL85 also published several PN distances by the same method, and we included their results in Table 2.

In Figure 4 we plot the data of Table 2 on the $\tau - \log \mu$ plane, drawing also the CKS and the SSV distance scales (note that the scales of Figures 3 and 4 are different). It is interesting to note that the best data points, those of the PNe whose distances have been determined via parallax or cluster membership, follow very well the SSV calibration, and they are less compatible with that of CKS. Naturally, the CKS calibration was based principally on reddening and expansion distances, since very few parallaxes were available at that time, and we can see that the thinning sequence determined by the data points relative to expansion or reddening distances is compatible with the CKS calibration (but these individual distances have much lower reliability than the parallaxes and cluster memberships represented by the filled symbols). While the SSV seems to be the best statistical scale to be used for Galactic PNe, its preference, for optically thick PNe, over the CKS scale is based only on one data point (the

parallax at $\tau < 2.1$). But let us recall here that the filled symbols *are not* the calibrators of the SSV scale, rather they are the Galactic PNe with best individual distances to date, used for comparison, while the calibration is based on ~ 70 data points whose errorbars would be smaller than the symbols.

In Figure 5 we show the direct comparison of the individual PN distances and those from the SSV calibration, where the correspondence of the parallax and cluster membership individual distances with the SSV distances is remarkable. It is worth noting that the two lower-left filled circles, those for which the parallax and statistical distances do not coincide within 30%, are A 7 and A 31; both are very large nebulae, whose diameters are larger than the radio beam used to detect the 5 GHz flux (Milne 1979), and whose flux densities are deemed to be uncertain. In Figure 6 we show the distribution of the relative differences of the SSV and individual distances versus τ for the four methods of deriving individual distances. The thin vertical lines represent the $\tau=2.1$ and $\tau=3.1$, i.e., the thick-to-thin PN transition for the CKS and SSV scales. We could conclude that the SSV scale fails to reproduce the individual distances for PNe around the transition between thick to thin, but this failure seems to pertain only to the comparison with expansion and reddening distances, and it does not occur for the comparison with parallax and cluster membership distances.

5. Comparison of Statistical Distance Scales

We compare the relative merits of the new SSV scale, calibrated on Magellanic Cloud PNe, in relation to other distance scales in the literature. We compare the statistical distances from different methods to individual Galactic PN distances, by using only the best individual PN distances of Table 2, those from parallax and cluster membership. We also calculate the distances to all LMC and SMC PNe using the statistical methods, then we compare the resulting averages with the actual distances to the Clouds. It is worth recalling that all old scales have been calibrated with Galactic or Bulge PNe, thus we expect a lower reproducibility of the Magellanic Cloud distances.

For all scales we give in Table 3: in column (1) the reference, in column (2) the statistical method,

in column (3) the correlation coefficient between statistical and individual PN distances, in column (4) the mean relative difference between the statistical and individual distances, in column (5) the relative difference between the median distances to Large Magellanic Cloud PNe and the actual LMC distance, in column (6) the same relative difference, but for the SMC PNe. Statistical distance scales in the literature use in this comparison are those by CKS, vdSZ, Z95, SB96, and BL01.

The statistical scheme that best compares with the best individual distances is the SSV scale, with higher ($R_{xy}=0.99$) correlation and lower median difference between statistical and individual distances than any other scale, and best reproduces the Magellanic Cloud distances. This is hardly a surprise, since for the first time it was possible to calibrate a distance scale with absolute calibrators from the Magellanic Clouds. By comparison, the correlation coefficients between the distances from the CKS, vdSZ, Z95, SB96, and BL01 scales are always lower, and the median of the relative differences are higher.

We also want to test whether PN distances derived with other distance scales, if recalibrated with the Magellanic Cloud PNe, would compare better than the SSV scale to the best individual distances of Galactic PNe. First, we consider the relation between the brightness temperature and the linear nebular radius, which vdSZ calibrated with Galactic bulge PNe. Our new calibration of the relation is

$$\log D(T_b) = 3.49 - 0.35 \log \theta - 0.32 \log F, \quad (5)$$

based on a fit of the $\log T_b - \log R_{PN}$ relation ($R_{PN} = (\theta D)/206265$). We also calibrate the $\log M_{ion} - \log R_{PN}$ relation as in Maciel & Pottasch (1980), Z95, and BL01, and found, by assuming that the filling factor is 0.6,

$$\log D(M_{ion}) = 3.45 - 0.34 \log \theta - 0.33 \log F. \quad (6)$$

Finally, we also recalibrate with the Magellanic Cloud PNe the relation between the surface brightness, $I=F/(\pi \theta^2)$, and R_{PN} , as in SB96, and obtained:

$$\log D(I) = 3.68 - 0.50 \log \theta - 0.25 \log F. \quad (7)$$

The possibility of building a distance scale based on a $\log I - \log R_{PN}$ calibration was mentioned by Stanghellini et al. (2002), and also used by Jacoby (2002).

All three relations used to derive the distance scales in Eqs. (5), (6), and (7) have high correlation coefficients ($R_{xy} \sim 0.8$). In these relations, excluding the bipolar PNe does not change the coefficients by more than 5%, thus their exclusion as calibrators is irrelevant.

Using the scales in Eqs. (5), (6), and (7) we have calculated the distances for those Galactic PNe whose individual distances are known either through a trigonometric or spectroscopic parallax, or by cluster membership. In Table 3 we give the comparison between these newly calibrated scales and the individual distances of PNe. We also give the estimates for the LMC and SMC distances, and we infer that the SSV scale is superior to all other scales here recalibrated with the Magellanic Cloud PNe as well. We then plot in Figure 7 the relative difference between the statistical and individual distances for the scales recalibrated with Magellanic Cloud PNe. The filled symbols represent the SSV scale, triangles are the distances from the T_b - R_{PN} relation (Eq. 5), crosses represent the $\log M_{ion} - \log R_{PN}$ scale (Eq. 6), pentagons are the distances from Eq. (7), based on the $\log I - \log R_{PN}$ relation. We see that the SSV scale is the best possible Galactic statistical distance scale with the calibrators and comparisons available to date. Since the $\log I - \log R_{PN}$ relation works for bipolar PNe, it might be used to determine the distance to bipolar PNe instead of the SSV scale.

6. Conclusion

The wealth of new data available that describe the physical parameters of Magellanic PNe has allowed us to check and re-calibrate the Shklovsky/Daub/CKS statistical distance scale, which is most commonly used in the literature, and provide distances of 645 Galactic PNe following the new distance scale calibration (Table 1). To calculate the SSV distance for other PNe, or for the same PNe but using other parameters than those in CKS, given θ and F , the 5 GHz flux, one can use the following equations:

$$\log D_{\text{SSV}} = 3.06 + 0.37 \log \theta - 0.68 \log F, \tau < 2.1 \quad (8a),$$

$$\log D_{\text{SSV}} = 3.79 - 0.6 \log \theta - 0.2 \log F, \tau > 2.1 \quad (8b).$$

If the 5 GHz flux is not available for the given PN, one can use Eq. (6) in CKS to derive the equivalent 5 GHz flux from the $H\beta$ flux.

In this paper we have used recent data on PNe in the Magellanic Clouds to construct a set of calibrators for which the distances are known to high absolute accuracy ($\sim 10\%$), and for which the dispersion among the distances is extraordinarily small (a few percent). Furthermore, the great distance of these nebulae allows us to establish a distance scale factor that is insensitive to uncertainties in distances to Galactic PNe that are drawn from a heterogeneous, nearby (few hundred pc) sample; a local sample has generally been necessary given the limited range over which many independent distance methods (notably trigonometric and expansion parallaxes) can provide accurate distances. In addition, we use consistent and reliable means to determine angular sizes (from photometric radii), and the $H\beta$ fluxes and extinction constants, derived from *HST* calibrations, are among the most reliable in the literature. There has never been a better set of calibrators for statistical distance determinations. For comparison, we selected Galactic PNe where the independent distances are the best available (including recently published data), and we evaluated the reliability of various independent distance methods by the degree to which they are consistent with our distance scale.

With this study we show that: (1) the distance scale as calibrated from the Magellanic Cloud PNe is very similar to that derived by CKS; (2) our revised distance scale agrees superbly with the most accurate distances measured for individual Galactic PNe. We also show that other methods of statistical distance determination generally do not yield results that are better than this statistical method; (3) the distance scale does not work for PNe with bipolar morphology, and we believe this is because progenitors of bipolars are often not fully ionized during the course of PN evolution (the $\log I - \log R_{\text{PN}}$ relation could be used instead for these PNe); (4) with the Magellanic Cloud cali-

bration we provide a more robust physical basis for why the Shklovsky/Daub distance scale works, despite wide variations in the expected ionized mass; we also show that the recalibration of other distance scales with Magellanic Cloud PNe might not work as well as the recalibrated Shklovsky/Daub distance scale; (5) we point out that the dispersion in the distance scale is an inherent property of the method, and cannot be reduced significantly by using better calibrators; (6) the radiation-bounded sequence for Magellanic Cloud PNe may terminate at higher surface brightness than previously derived. It seems that the new sequence and the radiation bounded to density bounded transition does not depend on metallicity very much, as it is the same for the LMC and the SMC PNe; the best available data show that the Magellanic Cloud calibration of this sequence is entirely consistent with Galactic PNe.

Many thanks to Bruce Balick for scientific discussion on the importance of the PN distance scale, and an anonymous referee for giving suggestions that improved the paper. Letizia Stanghellini is grateful to the Aspen Center for Physics for their hospitality on July 2006, when parts of this paper were completed.

REFERENCES

- Acker, A., Marcout, J., Ochsenbein, F., Stenholm, B., & Tylenda, R. 1992, Garching: European Southern Observatory, 1992
- Alves, D. R., Bond, H. E., & Livio, M. 2000, *AJ*, 120, 2044 (ABL00)
- Benedict, G. F., et al. 2002, *AJ*, 123, 473
- Bensby, T., & Lundström, I. 2001, *A&A*, 374, 599 (BL01)
- Cahn, J. H., Kaler, J. B., & Stanghellini, L. 1992, *A&AS*, 94, 399 (CKS)
- Chen, L., Hou, J. L., & Wang, J. J. 2003, *AJ*, 125, 1397 (CHW03)
- Ciardullo, R., Bond, H. E., Sipior, M. S., Fullton, L. K., Zhang, C.-Y., & Schaefer, K. G. 1999, *AJ*, 118, 488 (C99)

- Crowl, H. H., Sarajedini, A., Piatti, A. E., Geisler, D., Bica, E., Clariá, J. J., & Santos, J. F. C. 2001, *AJ*, 122, 220
- Daub, C. T. 1982, *ApJ*, 260, 612 (D82)
- Feast, M. W. 1989, Recent Developments of Magellanic Cloud Research, ed. K. S. de Boer, F. Spite, & G. Stasinska (Paris: Observatoire de Paris), 75
- Freeman, K. C., Illingworth, G., & Oemler, A. 1983, *ApJ*, 272, 488
- Freedman, W. L., et al. 2001, *ApJ*, 553, 47
- Gathier, R., Pottasch, S. R., & Pel, J. W. 1986, *A&A*, 157, 171 (GPP86)
- Gomez, Y., Rodriguez, L. F., & Moran, J. M. 1993, *ApJ*, 416, 620 (GRM93)
- Hajian, A. R., Terzian, Y., & Bignell, C. 1993, *AJ*, 106, 1965 (HTB93)
- Hajian, A. R., Terzian, Y., & Bignell, C. 1995, *AJ*, 109, 2600 (HTB95)
- Hajian, A. R., & Terzian, Y. 1996, *PASP*, 108, 258 (HT96)
- Harris, H. C., et al. 2007, *AJ*, 133, 631 (Hea07)
- Jacoby, G. H., Morse, J. A., Fullton, L. K., Kwitter, K. B., & Henry, R. B. C. 1997, *AJ*, 114, 2611
- Jacoby, G. H., Feldmeier, J. J., Claver, C. F., Garnavich, P. M., Noriega-Crespo, A., Bond, H. E., & Quinn, J. 2002, *AJ*, 124, 3340
- Kaler, J. B., & Lutz, J. H. 1985, *PASP*, 97, 700 (KL85)
- Liller, M. H., & Liller, W. 1968, *IAU Symp.* 34: Planetary Nebulae, 34, 38 (LL68)
- Maciel, W. J., & Pottasch, S. R. 1980, *A&A*, 88, 1
- Maciel, W. J. 1984, *A&AS*, 55, 253
- Mermilliod, J.-C., Clariá, J. J., Andersen, J., Piatti, A. E., & Mayor, M. 2001, *A&A*, 375, 30
- Milne, D. K. 1979, *A&AS*, 36, 227
- Monaco, L., Pancino, E., Ferraro, F. R., & Bellazzini, M. 2004, *MNRAS*, 349, 1278
- Mould, J. R., et al. 2000, *ApJ*, 529, 786
- Palen, S., Balick, B., Hajian, A. R., Terzian, Y., Bond, H. E., & Panagia, N. 2002, *AJ*, 123, 2666 (Pea02)
- Pauldrach, A., Puls, J., Kudritzki, R. P., Mendez, R. H., & Heap, S. R. 1988, *A&A*, 207, 123
- Russell, S. C. & Bessell, M. S. 1989, *ApJS*, 70, 865
- Russell, S. C. & Dopita, M. A. 1990, *ApJS*, 74, 93
- Sabbadin, F., Turatto, M., Cappellaro, E., Benetti, S., & Ragazzoni, R. 2004, *A&A*, 416, 955 (Sea04)
- Schneider, S. E., & Buckley, D. 1996, *ApJ*, 459, 606 (SB96)
- Shaw, R. A., Stanghellini, L., Mutchler, M., Balick, B., & Blades, J. C. 2001, *ApJ*, 548, 727
- Shaw, R. A., Stanghellini, L., Villaver, E., & Mutchler, M. 2006, *ApJS*, 167, 201
- Shklovsky, I. S. 1956a, *Astr. Zh.*, 33, 222
- Shklovsky, I. S. 1956b, *Astr. Zh.*, 33, 315
- Stanghellini, L., Shaw, R. A., Mutchler, M., Palen, S., Balick, B., & Blades, J. C. 2002, *ApJ*, 575, 178
- Stanghellini, L., Shaw, R. A., Balick, B., Mutchler, M., Blades, J. C., & Villaver, E. 2003, *ApJ*, 596, 997
- van der Marel, R. P. & Cioni, M. L. 2001, *AJ*, 122, 1807
- van de Steene, G. C., & Zijlstra, A. A. 1995, *A&A*, 293, 541 (vdSZ)
- Villaver, E., García-Segura, G., & Manchado, A. 2002a, *ApJ*, 571, 880
- Villaver, E., Manchado, A., & García-Segura, G. 2002b, *ApJ*, 581, 1204
- Westerlund, B. E. 1997, *The Magellanic Clouds* (Cambridge: Cambridge Univ. Press)

Winters, J. M., Le Bertre, T., Jeong, K. S.,
Helling, C., & Sedlmayr, E. 2000, A&A, 361,
641

Zhang, C. Y. 1995, ApJS, 98, 659 (Z95)

TABLE 1
CATALOG OF GALACTIC PN DISTANCES

Name	τ	θ "	F ^a	D _{SSV} [pc]
NGC40	3.46	18.20	0.460	1249
NGC246	5.31	112.00	0.248	475
NGC650	5.24	69.20	0.110	746
NGC1360	5.82	192.00	0.222	351
NGC1501	4.08	25.90	0.224	1167
NGC1514	4.59	50.20	0.262	760
NGC1535	3.31	9.20	0.166	2305
NGC2022	3.62	9.70	0.091	2518
NGC2346	4.54	27.30	0.086	1369
NGC2371	4.33	21.80	0.090	1554
NGC2392	3.93	22.40	0.237	1259
NGC2438	4.83	35.20	0.073	1215
NGC2440	3.42	16.40	0.411	1359
NGC2452	3.81	9.40	0.055	2838
NGC2610	4.58	17.20	0.031	2215
NGC2792	3.16	6.50	0.116	3050
NGC2818	4.69	20.00	0.033	1998
NGC2867	2.93	8.00	0.299	2228
NGC2899	4.97	45.00	0.086	1014
NGC3132	3.94	22.50	0.230	1263
NGC3195	4.66	20.00	0.035	1975
NGC3211	3.51	8.00	0.080	2901
NGC3242	3.22	18.60	0.835	1094
NGC3587	5.64	100.00	0.091	621
NGC3699	4.48	22.40	0.067	1620
NGC3918	2.62	9.40	0.857	1639
NGC4071	5.18	31.50	0.026	1596
NGC4361	4.45	40.50	0.230	887
NGC5189	4.59	70.00	0.507	546
NGC5307	3.22	6.30	0.095	3235
NGC5873	3.08	3.50	0.041	5445
NGC5882	2.77	7.00	0.334	2362
NGC5979	2.74	4.00	0.117	4075
NGC6026	4.72	16.90	0.022	2398
NGC6058	5.03	13.20	0.007	3538
NGC6072	4.43	35.00	0.181	1017
NGC6153	2.98	12.30	0.632	1482
NGC6210	3.01	8.10	0.256	2282
NGC6302	2.77	22.30	3.403	741

TABLE 1—*Continued*

Name	τ	θ "	F ^a	D _{SSV} [pc]
NGC6309	3.06	6.90	0.167	2736
NGC6326	3.30	6.00	0.073	3511
NGC6337	4.19	23.50	0.143	1354
NGC6369	2.59	14.00	2.002	1089
NGC6439	2.67	2.50	0.053	6330
NGC6445	3.48	16.60	0.368	1380
NGC6543	2.59	9.40	0.899	1623
NGC6563	4.42	21.50	0.070	1646
NGC6565	3.29	4.50	0.042	4660
NGC6567	2.68	4.40	0.161	3610
NGC6572	2.16	7.20	1.429	1736
NGC6578	2.65	4.30	0.166	3638
NGC6620	3.40	2.50	0.010	8836
NGC6629	2.93	7.50	0.266	2372
NGC6720	4.10	34.60	0.384	880
NGC6741	2.49	3.90	0.197	3728
NGC6751	3.85	10.50	0.063	2585
NGC6765	4.91	19.00	0.018	2334
NGC6772	4.74	32.40	0.076	1266
NGC6778	3.66	7.90	0.055	3150
NGC6781	4.54	53.00	0.323	706
NGC6803	2.52	2.80	0.094	5273
NGC6804	3.84	15.70	0.142	1726
NGC6807	2.17	1.00	0.027	12550
NGC6818	3.04	9.10	0.304	2055
NGC6826	3.20	12.70	0.404	1590
NGC6842	4.25	23.70	0.126	1380
NGC6852	4.59	14.00	0.020	2736
NGC6853	4.94	170.00	1.325	264
NGC6879	3.10	2.50	0.020	7692
NGC6881	2.30	2.50	0.124	5340
NGC6884	2.49	3.80	0.186	3830
NGC6886	2.77	3.80	0.098	4354
NGC6891	3.00	5.10	0.103	3613
NGC6894	4.50	22.00	0.061	1669
NGC6905	4.42	20.20	0.062	1751
NGC7008	4.53	42.80	0.217	869
NGC7009	3.03	14.10	0.735	1325
NGC7026	2.91	7.50	0.277	2352

TABLE 1—*Continued*

Name	τ	θ "	F ^a	D _{SSV} [pc]
NGC7048	4.91	27.50	0.037	1613
NGC7094	5.72	47.50	0.017	1358
NGC7139	5.30	38.00	0.029	1396
NGC7293	5.70	402.00	1.292	159
NGC7354	2.83	10.00	0.597	1698
NGC7662	2.57	7.70	0.634	1962
IC289	3.81	18.40	0.212	1448
IC351	3.15	3.50	0.035	5620
IC972	5.51	23.50	0.007	2488
IC1295	5.42	54.10	0.045	1034
IC1297	2.85	3.50	0.069	4908
IC1454	5.95	17.00	0.001	4207
IC1747	3.12	6.50	0.128	2991
IC2003	2.97	3.30	0.047	5489
IC2120	4.24	23.50	0.126	1388
IC2149	2.36	4.20	0.309	3258
IC2165	2.50	4.00	0.202	3653
IC2448	3.17	5.00	0.067	3985
IC2553	2.77	4.50	0.137	3679
IC2621	2.10	2.50	0.197	4867
IC3568	3.64	9.00	0.075	2738
IC4191	3.06	7.00	0.170	2703
IC4406	3.56	10.00	0.110	2381
IC4593	3.25	6.40	0.092	3225
IC4634	2.76	4.20	0.122	3924
IC4637	3.42	9.30	0.132	2396
IC4642	3.66	8.30	0.060	3006
IC4663	3.66	7.20	0.045	3467
IC4673	3.56	7.40	0.060	3220
IC4699	3.10	2.50	0.020	7692
IC4732	2.83	2.50	0.037	6801
IC4776	2.88	3.50	0.065	4966
IC5148	5.71	60.00	0.028	1068
IC5217	2.98	3.40	0.048	5369
A1	5.55	23.50	0.006	2534
A2	5.62	15.50	0.002	3967
A3	6.12	30.00	0.003	2585
A4	5.43	10.00	0.001	5621
A5	6.80	63.70	0.003	1658

TABLE 1—*Continued*

Name	τ	θ "	F ^a	D _{SSV} [pc]
A6	6.45	93.00	0.012	967
A7	6.28	382.00	0.305	218
A8	5.15	30.00	0.026	1648
A9	6.02	18.50	0.001	3999
A10	5.20	10.00	0.002	5075
A11	5.01	16.00	0.010	2901
A12	4.58	18.50	0.036	2058
A13	6.47	76.30	0.008	1191
A14	5.38	16.40	0.004	3353
A15	5.67	17.00	0.002	3691
A16	6.59	70.50	0.005	1363
A17	5.79	21.40	0.003	3100
A18	5.50	36.60	0.017	1588
A19	6.12	33.50	0.003	2310
A20	5.78	33.50	0.007	1978
A23	5.63	27.00	0.007	2289
A24	6.54	177.40	0.036	530
A26	5.82	20.00	0.002	3376
A28	7.13	134.00	0.005	920
A30	6.85	63.50	0.002	1702
A31	6.97	486.00	0.102	235
A32	6.05	67.00	0.016	1118
A33	6.71	134.00	0.014	758
A34	6.79	145.00	0.013	728
A35	6.37	386.00	0.255	225
A36	5.89	183.50	0.174	379
A39	6.72	87.00	0.006	1175
A40	5.76	17.00	0.002	3859
A41	4.83	9.20	0.005	4644
A43	5.76	40.00	0.011	1634
A44	5.50	28.00	0.010	2074
A46	5.91	31.70	0.005	2211
A50	5.86	13.50	0.001	5091
A51	5.19	33.50	0.029	1503
A53	4.05	15.50	0.086	1924
A54	6.10	28.00	0.002	2736
A55	5.58	24.00	0.006	2519
A59	5.61	43.00	0.018	1425
A60	5.70	37.00	0.011	1721

TABLE 1—*Continued*

Name	τ	θ "	F ^a	D _{SSV} [pc]
A62	4.70	80.50	0.522	499
A65	6.45	54.00	0.004	1671
A66	6.09	133.40	0.058	572
A67	5.82	33.50	0.007	2011
A69	5.01	11.00	0.005	4206
A70	5.17	21.00	0.012	2376
A71	5.48	79.00	0.083	729
A72	6.00	63.70	0.016	1151
A73	5.86	36.60	0.007	1875
A75	5.28	28.50	0.017	1845
A77	4.15	32.90	0.308	949
A78	6.37	53.50	0.005	1622
A79	5.12	27.10	0.022	1801
A80	6.59	54.80	0.003	1752
A81	5.92	16.50	0.001	4283
A82	6.09	40.50	0.005	1887
A84	6.05	47.50	0.008	1579
AGCAR	3.56	17.80	0.348	1338
Ap1-11	4.41	6.00	0.006	5847
Ap1-12	4.26	6.00	0.019	4610
Ap2-1	3.53	16.40	0.320	1429
Ap2-1	4.58	50.00	0.262	762
Ba-1	5.05	19.00	0.013	2483
BD+30	2.10	4.00	0.511	3034
BIM	3.10	2.30	0.017	8354
BV-1	4.99	20.80	0.018	2211
Cn1-5	3.05	3.50	0.044	5369
Cn2-1	2.35	1.70	0.052	8008
Cn3-1	2.57	2.50	0.067	6040
CRL618	3.33	6.00	0.067	3572
DdDm-1	2.22	0.50	0.006	25700
Fg-1	3.67	8.00	0.055	3127
Ha1-1	3.14	1.20	0.004	16400
Ha1-3	2.79	7.90	0.405	2113
Ha1-8	2.57	1.70	0.031	8881
Ha1-11	3.44	3.00	0.013	7515
Ha1-14	3.30	3.30	0.022	6389
Ha1-15	3.17	2.20	0.013	9052
Ha1-17	2.13	0.50	0.006	25700

TABLE 1—*Continued*

Name	τ	θ "	F ^a	D _{SSV} [pc]
Ha1-20	2.56	2.00	0.044	7514
Ha1-23	2.35	1.40	0.035	9750
Ha1-24	3.70	4.30	0.015	5892
Ha1-27	3.18	2.60	0.018	7673
Ha1-33	2.82	1.40	0.012	12060
Ha1-39	2.37	0.90	0.014	15290
Ha1-40	2.36	1.90	0.063	7200
Ha1-41	3.86	4.80	0.013	5686
Ha1-42	2.92	2.90	0.040	6126
Ha1-43	3.18	1.50	0.006	13300
Ha1-54	2.13	1.00	0.029	12340
Ha1-59	3.94	3.00	0.004	9421
Ha1-60	3.11	1.90	0.011	10170
Ha1-65	3.21	2.60	0.017	7780
Ha1-66	3.86	3.30	0.006	8284
Ha1-67	3.51	3.00	0.011	7770
Ha2-1	2.68	2.80	0.065	5677
Ha2-7	3.29	2.10	0.009	10020
Ha2-10	2.30	1.00	0.020	13330
Ha2-10	2.42	1.00	0.015	14060
Ha2-15	3.76	1.70	0.002	15360
Ha2-16	4.91	8.40	0.003	5268
Ha2-17	3.10	1.80	0.010	10720
Ha2-20	2.95	1.90	0.016	9447
Ha2-24	3.21	2.30	0.013	8814
Ha2-25	3.68	2.20	0.004	11460
Ha2-33	4.11	4.00	0.005	7655
Ha2-41	4.26	3.80	0.003	8632
Ha2-43	3.49	4.50	0.026	5114
Ha3-29	3.90	6.00	0.018	4646
Ha4-1	3.83	1.50	0.001	18050
Hb-4	2.18	2.50	0.166	5037
Hb-5	2.81	10.00	0.620	1685
Hb-7	2.73	2.00	0.030	8109
Hb-8	3.49	2.50	0.008	9239
He1-5	5.39	18.00	0.005	3081
He1-6	4.39	11.20	0.020	3119
He2-5	2.49	1.50	0.029	9702
He2-7	4.63	22.30	0.047	1744

TABLE 1—*Continued*

Name	τ	θ "	F ^a	D _{SSV} [pc]
He2-11	3.98	32.50	0.445	888
He2-15	3.73	11.90	0.105	2165
He2-21	2.56	1.20	0.016	12490
He2-26	4.56	19.00	0.040	1983
He2-28	3.70	5.00	0.020	5075
He2-29	3.91	7.00	0.024	3999
He2-35	3.02	2.50	0.024	7416
He2-36	3.81	11.00	0.075	2427
He2-37	4.37	11.50	0.023	3004
He2-50	4.09	5.90	0.011	5151
He2-51	3.15	4.50	0.057	4384
He2-63	2.88	1.50	0.012	11570
He2-73	2.32	2.00	0.076	6733
He2-85	2.97	5.10	0.112	3555
He2-99	4.21	8.50	0.018	3770
He2-102	3.39	4.50	0.033	4891
He2-103	4.35	10.00	0.018	3419
He2-105	4.84	15.50	0.014	2764
He2-107	3.19	5.00	0.065	4009
He2-108	3.56	5.50	0.033	4336
He2-109	3.54	3.70	0.016	6373
He2-111	3.30	6.00	0.073	3511
He2-112	3.41	7.30	0.082	3050
He2-114	5.09	18.30	0.011	2626
He2-116	5.58	25.50	0.007	2369
He2-119	4.47	26.40	0.094	1372
He2-120	4.45	13.50	0.026	2653
He2-123	2.28	2.30	0.110	5750
He2-125	2.65	1.50	0.020	10410
He2-132	4.10	8.90	0.025	3434
He2-138	2.81	3.50	0.076	4813
He2-141	3.57	6.90	0.051	3469
He2-142	2.30	1.80	0.065	7400
He2-143	2.35	2.60	0.120	5250
He2-146	3.42	11.00	0.186	2024
He2-149	3.12	1.50	0.007	12970
He2-152	2.79	5.50	0.196	3036
He2-153	5.17	6.50	0.001	7744
He2-155	3.48	7.30	0.070	3148

TABLE 1—*Continued*

Name	τ	θ "	F ^a	D _{SSV} [pc]
He2-157	2.48	1.50	0.030	9637
He2-158	3.17	1.00	0.003	19890
He2-159	3.60	5.00	0.025	4853
He2-161	3.80	5.00	0.016	5313
He2-163	5.07	10.00	0.003	4772
He2-164	3.42	8.00	0.097	2791
He2-165	5.20	25.00	0.016	2023
He2-169	3.74	10.90	0.086	2374
He2-175	3.21	3.30	0.027	6141
He2-180	2.23	0.90	0.019	14350
He2-186	2.63	1.50	0.021	10350
He2-262	2.60	1.60	0.026	9540
He2-429	2.41	2.10	0.069	6659
He2-432	2.17	1.10	0.033	11420
He2-433	3.66	4.00	0.014	6231
He2-435	3.19	2.40	0.015	8349
He2-453	4.52	11.20	0.015	3313
Hf2-1	3.99	4.70	0.009	6165
Hu1-1	3.03	2.50	0.023	7460
J320	3.39	3.60	0.021	6120
J900	2.51	3.00	0.110	4903
Jn-1	7.05	166.00	0.010	716
K1-1	5.22	21.70	0.011	2362
K1-3	3.88	46.00	1.117	599
K1-4	4.93	23.00	0.025	1943
K1-7	5.76	17.00	0.002	3859
K1-8	5.02	39.50	0.059	1183
K1-12	5.14	18.50	0.010	2659
K1-13	5.67	83.00	0.059	758
K1-14	6.20	23.50	0.001	3413
K1-16	5.07	47.00	0.076	1013
K1-20	5.95	17.00	0.001	4207
K1-21	5.23	14.50	0.005	3535
K1-22	6.45	90.50	0.012	997
K1-32	6.00	29.50	0.003	2479
K2-1	5.92	66.00	0.021	1071
K2-2	6.50	207.00	0.054	446
K2-4	6.37	343.00	0.202	253
K2-5	4.88	12.30	0.008	3561

TABLE 1—*Continued*

Name	τ	θ "	F ^a	D _{SSV} [pc]
K3-1	3.70	2.50	0.005	10150
K3-2	2.41	1.40	0.031	9991
K3-3	3.47	5.50	0.041	4144
K3-4	4.10	8.10	0.021	3762
K3-5	4.52	5.00	0.003	7416
K3-7	3.14	3.20	0.030	6116
K3-9	3.89	3.80	0.007	7280
K3-11	2.72	1.50	0.017	10800
K3-13	2.63	1.90	0.034	8156
K3-14	2.32	0.50	0.005	26880
K3-16	3.37	2.00	0.007	10910
K3-17	2.74	7.40	0.398	2205
K3-18	3.09	2.00	0.013	9600
K3-23	3.03	1.50	0.008	12460
K3-24	3.17	3.10	0.026	6405
K3-27	4.63	8.20	0.006	4752
K3-30	2.70	1.70	0.023	9427
K3-37	2.60	1.30	0.017	11760
K3-38	2.52	1.50	0.025	9978
K3-40	2.90	2.00	0.020	8794
K3-41	2.17	0.25	0.002	50140
K3-48	3.02	3.00	0.034	6201
K3-55	2.87	4.10	0.090	4231
K3-57	2.83	3.20	0.060	5325
K3-58	2.87	2.40	0.031	7221
K3-61	3.41	3.00	0.014	7405
K3-63	3.23	3.50	0.029	5836
K3-65	3.80	2.50	0.004	10610
K3-66	2.43	1.10	0.018	12860
K3-67	3.73	7.50	0.042	3430
K3-68	4.46	6.00	0.005	6002
K3-70	2.63	0.80	0.006	19390
K3-72	5.55	11.50	0.001	5168
K3-77	3.32	3.80	0.027	5618
K3-78	3.05	2.20	0.017	8540
K3-82	4.32	12.50	0.030	2700
K3-83	3.59	2.50	0.006	9631
K3-87	3.90	3.00	0.004	9291
K3-90	3.77	4.50	0.014	5814

TABLE 1—*Continued*

Name	τ	θ "	F ^a	D _{SSV} [pc]
K3-91	4.82	5.00	0.001	8519
K3-92	4.93	6.50	0.002	6871
K3-94	4.26	5.00	0.005	6570
K4-16	3.48	1.50	0.003	15270
K4-30	2.51	1.30	0.021	11280
K4-39	2.65	1.00	0.009	15640
K4-41	2.78	1.50	0.015	11070
K4-45	3.25	4.50	0.046	4576
K4-47	4.31	3.90	0.003	8609
K4-48	2.54	1.10	0.014	13520
K4-58	4.30	5.00	0.005	6696
K4-60	2.85	10.00	0.560	1719
LoTr5	4.29	5.30	0.006	6321
M1-1	3.58	3.00	0.009	8002
M1-4	2.28	2.00	0.084	6600
M1-7	3.77	4.40	0.013	5963
M1-8	4.17	9.20	0.023	3423
M1-9	2.20	1.10	0.030	11580
M1-13	3.82	5.00	0.015	5375
M1-14	2.61	2.40	0.056	6416
M1-16	2.51	1.50	0.028	9770
M1-17	2.72	1.50	0.017	10800
M1-18	5.82	15.20	0.001	4433
M1-19	2.42	1.30	0.026	10810
M1-22	4.01	3.00	0.003	9770
M1-25	2.59	2.30	0.055	6605
M1-27	3.01	4.00	0.063	4612
M1-28	4.04	7.40	0.020	4011
M1-29	2.82	4.10	0.102	4127
M1-31	2.93	3.50	0.057	5098
M1-32	2.96	3.80	0.064	4741
M1-33	2.38	1.90	0.060	7280
M1-34	3.93	5.60	0.015	5042
M1-35	2.68	2.60	0.057	6093
M1-39	2.20	2.00	0.100	6374
M1-41	4.22	38.00	0.350	848
M1-42	3.45	4.10	0.024	5512
M1-44	3.25	2.00	0.009	10320
M1-46	3.15	5.50	0.086	3580

TABLE 1—*Continued*

Name	τ	θ "	F ^a	D _{SSV} [pc]
M1-47	3.35	2.80	0.014	7718
M1-48	3.58	2.40	0.006	10030
M1-50	2.80	2.80	0.050	5983
M1-51	2.85	7.50	0.319	2287
M1-52	3.90	4.00	0.008	6969
M1-53	2.83	3.00	0.053	5674
M1-54	3.65	6.50	0.038	3813
M1-57	3.01	4.20	0.069	4398
M1-58	2.83	3.20	0.060	5325
M1-59	2.16	2.30	0.148	5419
M1-60	2.11	1.30	0.052	9407
M1-63	3.24	2.10	0.010	9771
M1-64	5.08	8.50	0.002	5640
M1-65	2.77	1.80	0.022	9191
M1-66	2.12	1.40	0.059	8773
M1-67	4.76	60.20	0.250	688
M1-73	2.76	2.50	0.043	6600
M1-75	3.87	7.00	0.026	3929
M1-77	3.41	4.00	0.025	5549
M1-79	4.68	15.00	0.019	2652
M1-80	3.41	4.00	0.025	5549
M2-2	2.96	3.50	0.054	5153
M2-7	3.96	4.00	0.007	7157
M2-8	2.90	1.90	0.018	9262
M2-9	4.64	23.00	0.048	1705
M2-11	2.56	1.40	0.021	10750
M2-13	2.29	0.80	0.013	16610
M2-15	3.40	2.90	0.013	7623
M2-16	3.07	2.70	0.025	7035
M2-17	3.81	4.00	0.010	6664
M2-18	2.18	0.80	0.017	15740
M2-19	3.25	2.50	0.014	8261
M2-21	2.59	1.50	0.023	10160
M2-22	3.41	2.60	0.010	8546
M2-23	3.04	4.40	0.070	4262
M2-24	4.19	3.40	0.003	9347
M2-26	3.99	3.50	0.005	8294
M2-27	2.14	1.00	0.029	12400
M2-28	3.29	2.20	0.010	9540

TABLE 1—*Continued*

Name	τ	θ "	F ^a	D _{SSV} [pc]
M2-29	3.59	2.80	0.008	8632
M2-30	3.06	2.00	0.014	9444
M2-33	2.87	2.00	0.021	8668
M2-36	3.27	3.40	0.025	6117
M2-38	3.90	4.00	0.008	6969
M2-39	3.11	1.60	0.008	12080
M2-40	2.87	2.50	0.033	6942
M2-42	3.06	2.00	0.014	9444
M2-44	3.07	4.00	0.054	4756
M2-45	2.47	3.20	0.139	4502
M2-46	3.81	2.20	0.003	12140
M2-47	3.14	4.10	0.049	4788
M2-48	2.73	1.60	0.019	10160
M2-50	3.51	2.30	0.006	10120
M2-51	4.58	19.60	0.041	1941
M2-52	4.15	7.00	0.014	4454
M2-53	4.56	10.00	0.011	3773
M2-54	2.10	0.50	0.008	24270
M2-55	4.93	20.00	0.019	2232
M3-1	3.72	5.60	0.024	4571
M3-2	4.32	3.80	0.003	8930
M3-3	4.42	6.10	0.006	5810
M3-4	4.90	6.90	0.002	6392
M3-5	3.62	3.40	0.011	7208
M3-6	2.87	4.10	0.091	4222
M3-7	3.14	3.10	0.028	6320
M3-8	3.12	2.70	0.022	7206
M3-9	3.91	8.40	0.035	3324
M3-10	2.55	1.60	0.029	9334
M3-11	3.67	3.60	0.011	6965
M3-12	3.29	2.70	0.015	7780
M3-14	3.24	3.60	0.030	5699
M3-16	3.41	3.30	0.017	6727
M3-17	2.88	1.50	0.012	11570
M3-19	3.88	3.50	0.006	7870
M3-20	2.60	2.00	0.040	7655
M3-22	3.64	3.20	0.009	7714
M3-23	3.71	6.00	0.028	4253
M3-26	3.79	3.50	0.008	7550

TABLE 1—*Continued*

Name	τ	θ "	F ^a	D _{SSV} [pc]
M3-28	3.40	4.50	0.033	4903
M3-29	3.55	4.10	0.019	5794
M3-30	4.61	8.60	0.007	4484
M3-32	3.68	3.80	0.012	6627
M3-33	3.68	3.00	0.007	8389
M3-34	3.03	2.80	0.029	6649
M3-36	3.47	1.60	0.003	14250
M3-37	2.99	1.10	0.005	16610
M3-38	2.19	0.90	0.021	14060
M3-39	3.06	9.00	0.284	2098
M3-40	2.57	1.30	0.018	11630
M3-41	2.37	2.10	0.075	6556
M3-42	4.14	4.50	0.006	6901
M3-43	2.73	1.90	0.027	8528
M3-52	4.68	6.00	0.003	6648
M3-54	3.59	2.80	0.008	8632
M4-1	2.72	2.20	0.037	7344
M4-2	3.28	3.00	0.019	6966
M4-7	3.01	2.90	0.033	6366
M4-9	4.67	22.10	0.042	1794
M4-14	3.67	3.70	0.012	6756
M4-18	2.87	1.90	0.019	9133
Me1-1	2.73	2.40	0.043	6757
Me2-1	3.18	3.00	0.024	6665
My60	2.98	3.80	0.060	4803
MyCn18	3.18	6.30	0.106	3165
Mz1	4.04	12.90	0.061	2299
Mz2	3.85	11.50	0.075	2364
Mz3	3.00	12.70	0.649	1446
NA1	3.37	4.00	0.027	5464
PB2	2.35	1.50	0.040	9098
PB3	2.85	3.50	0.070	4893
PB4	3.25	5.60	0.071	3680
PB6	3.61	5.50	0.030	4419
PB8	2.98	2.50	0.026	7299
PB9	3.31	4.50	0.040	4706
PB10	3.11	4.00	0.050	4830
PC12	2.23	0.90	0.019	14350
PC14	3.21	3.50	0.030	5796

TABLE 1—*Continued*

Name	τ	θ "	F ^a	D _{SSV} [pc]
PC17	3.23	2.50	0.015	8180
PC19	2.49	1.40	0.025	10390
PC23	2.43	1.10	0.018	12860
PC24	3.14	2.50	0.018	7856
Pe1-5	2.71	5.50	0.233	2932
Pe1-6	3.11	3.60	0.040	5380
Pe1-11	4.01	4.50	0.008	6493
Pe1-12	4.63	6.00	0.003	6484
Pe1-13	4.21	3.50	0.003	9186
Pe1-15	3.25	2.50	0.014	8249
Pe1-17	3.91	3.50	0.006	7997
Pe1-19	3.51	2.20	0.006	10570
Pe1-20	3.14	3.20	0.029	6141
Pe1-21	3.39	4.30	0.030	5123
Pe2-12	4.10	2.50	0.002	12190
Pe2-15	2.88	1.30	0.009	13360
PHL932	6.92	135.00	0.009	828
Ps1	2.93	1.80	0.014	10000
Pu-1	5.80	33.00	0.007	2024
PW1	7.83	200.00	0.085	416
Sa1-8	3.46	2.80	0.011	8099
Sa2-21	5.82	20.00	0.002	3376
Sa2-22	4.15	4.00	0.004	7818
Sh1-89	4.53	19.00	0.043	1959
Sh1-118	5.80	57.50	0.021	1161
Sh2-71	5.18	49.80	0.066	1006
Sh2-207	5.12	100.00	0.300	489
Sh2-266	4.49	33.50	0.145	1091
Sn1	3.11	1.50	0.007	12890
Sp1	4.84	36.00	0.075	1192
Sp3	4.32	17.80	0.061	1895
Tc1	3.18	7.50	0.147	2669
Th2-A	3.95	11.50	0.060	2471
Th3-10	2.13	1.00	0.029	12330
Th3-19	2.98	1.00	0.004	18210
Th3-25	2.26	0.90	0.018	14500
Th3-26	3.64	3.30	0.010	7480
Th4-5	3.49	3.50	0.016	6573
VV-47	6.88	190.00	0.019	578

TABLE 1—*Continued*

Name	τ	θ "	F ^a	D _{SSV} [pc]
VV1-2	5.41	130.00	0.265	428
VV1-4	4.46	63.20	0.553	570
VV1-5	5.02	162.00	1.002	288
VV1-7	6.03	124.00	0.057	600
VV1-8	4.72	45.00	0.156	901
VV3-4	2.38	0.60	0.006	23040
Vy1-1	3.12	3.10	0.029	6281
Vy1-2	3.26	2.30	0.012	9002
Vy1-4	3.20	2.00	0.010	10100
Vy2-1	2.59	1.90	0.038	7997
Vy2-3	3.85	2.30	0.003	11820
We-1	5.38	9.50	0.001	5796
We-2	3.63	46.00	2.000	534
We-6	6.68	31.00	0.001	3233
We2-5	6.18	97.00	0.025	820
We2-262	6.80	65.00	0.003	1625
YM29	6.06	307.50	0.327	245

^aThis is the 5GHz flux when available, otherwise equivalent 5GHz flux from H β .

TABLE 2
INDIVIDUAL DISTANCES OF GALACTIC PNE

Name	D _{ind} [pc]	σ_D [pc]	τ	D _{CKS} [pc]	D _{SSV} [pc]	Method ^a	Ref ^b
A 7	676	$^{+267}_{-150}$	6.28	216	218	P	Hea07
A 24	521	$^{+112}_{-79}$	6.54	525	530	P	Hea07
A 31	568	$^{+131}_{-90}$	6.97	233	235	P	Hea07
BD+30	2680	810	2.1	1162	3034	E	HTB93
IC 289	2190	1630	3.81	1434	1448	R	KL85
IC 1747	2450	1150	3.12	2937	2991	R	KL85
IC 2448	1410	640	3.17	3947	3984	E	Pea02
HE 2-131	590	180	2.03	1413	3666	P	C99
K 1-14	3000	...	6.2	3378	3413	P	C99
K 1-22	1330	...	6.45	988	997	P	C99
Mz 2	2160	...	3.85	2341	2363	P	C99
NGC 2392	1600	130	3.93	1247	1258	E	LL68
NGC 2452	3570	560	3.81	2811	2838	R	GPP86
NGC 2792	1910	220	3.16	3021	3050	R	GPP86
NGC 2818	1855	200	4.69	1979	1998	CM	CHW03
NGC 3132	770	...	3.94	1251	1263	P	C99
NGC 3211	1910	500	3.51	2873	2901	R	GPP86
NGC 3242	420	160	3.22	1083	1094	E	HTB95
NGC 3918	2240	840	2.62	1010	1639	R	GPP86
NGC 5189	1730	530	4.59	540	546	R	GPP86
NGC 5315	2620	1030	1.94	1242	3177	R	GPP86
NGC 6210	1570	400	3.01	2025	2281	E	HTB95
NGC 6302	1600	600	2.77	525	741	E	GRM93
NGC 6565	1000	440	3.29	4616	4660	R	GPP86
NGC 6567	1680	170	2.68	2367	3610	R	GPP86
NGC 6572	703	95	2.16	705	1736	E	HTB95
NGC 6720	704	$^{+445}_{-196}$	4.1	872	880	P	Hea07
NGC 6741	1540	770	2.49	2047	3727	R	KL85
NGC 6853	379	$^{+54}_{-42}$	4.94	262	264	P	Hea07
NGC 6894	1090	110	4.5	1653	1669	R	KL85
NGC 7009	1400	...	3.03	1201	1325	E	Sea04
NGC 7026	1450	840	2.91	1902	2352	R	KL85
NGC 7027	790	...	1.46	273	632	P	HTB95
NGC 7293	219	$^{+27}_{-21}$	5.7	157	159	P	Hea07
NGC 7354	2460	1440	2.83	1271	1697	R	KL85
NGC 7662	790	750	2.57	1163	1962	E	HT96
PS 1	1.23e+4	600	2.93	8380	1.0e+4	CM	ABL00
Pw We 1	365	$^{+47}_{-37}$	7.83	141	416	P	Hea07
Sp 3	2380	...	4.32	1877	1895	P	C99

TABLE 2—*Continued*

Name	D_{ind} [pc]	σ_D [pc]	τ	D_{CKS} [pc]	D_{SSV} [pc]	Method ^a	Ref ^b
------	--------------------------	--------------------	--------	--------------------------	--------------------------	---------------------	------------------

^aP: parallax; CM: cluster membership; E: expansion; R: reddening.

^bABL00: Alves et al. 2000; CHW03: Chen et al. 2003; C99: Ciardullo et al. 1999; GPP86: Gathier et al. 1996; GRM93: Gomez et al. 1993; HTB93: Hajian et al. 1993; HTB95: Hajian et al. 1995; HT96: Hajian & Terzian 1996; Hea07: Harris et al. 2007; KL85: Kaler & Lutz 1985; LL68: Liller & Liller 1968; Pea02: Palen et al. 2002; Sea04: Sabbadin et al. 2004.

TABLE 3
COMPARISON OF STATISTICAL AND INDIVIDUAL DISTANCES

Ref.	Method	R_{xy}	$\langle \frac{\delta D}{D} \rangle_{\text{Gal}}$	$\frac{\langle D_{\text{stat}} \rangle - D_{\text{LMC}}}{D_{\text{LMC}}}$	$\frac{\langle D_{\text{stat}} \rangle - D_{\text{SMC}}}{D_{\text{SMC}}}$
SSV	$\mu\tau$	0.99	0.26	0.01	0.01
Old scales					
CKS	$\mu\tau$	0.97	0.32	0.04	0.05
vdSZ	$\log T_b - \log R_{\text{PN}}$	0.74	0.86	0.13	0.12
Z95	$\log M_{\text{ion}} - \log R_{\text{PN}}$	0.70	1.10	0.19	0.22
BL01	$\log M_{\text{ion}} - \log R_{\text{PN}}$	0.61	1.35	0.12	0.12
SB96	$\log I - \log R_{\text{PN}}$	0.95	0.46	0.02	0.02
LMC/SMC calibrations					
this paper	$\log T_b - \log R_{\text{PN}}$	0.82	0.74	0.07	0.02
this paper	$\log M_{\text{ion}} - \log R_{\text{PN}}$	0.80	0.72	0.11	0.08
this paper	$\log I - \log R_{\text{PN}}$	0.96	0.36	0.03	0.02

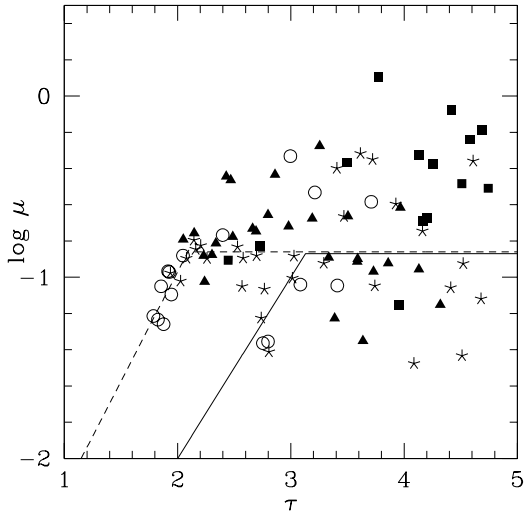


Fig. 1.— Plotted are $\log \mu$ versus τ for the sample of LMC PNe observed with the *HST*. Symbols indicate morphology types: Round (open circles), Elliptical (asterisks), Bipolar core (triangles) and Bipolar (squares). The thinning sequence is clearly defined for $\tau < 2.1$. The solid line reflect CKS calibration, the broken line is the new calibration (SSV).

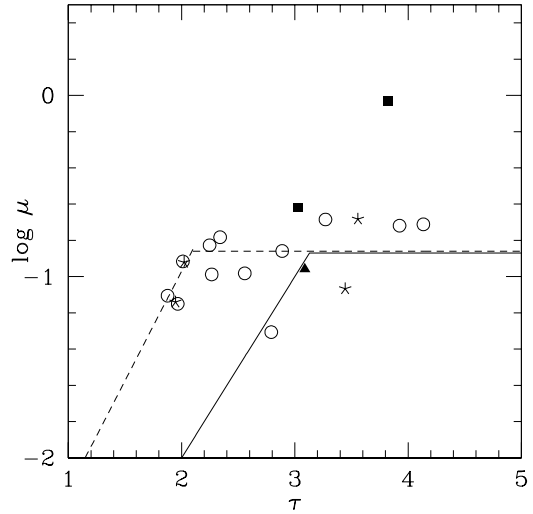


Fig. 2.— Same as in Figure 1, but for the SMC PNe.

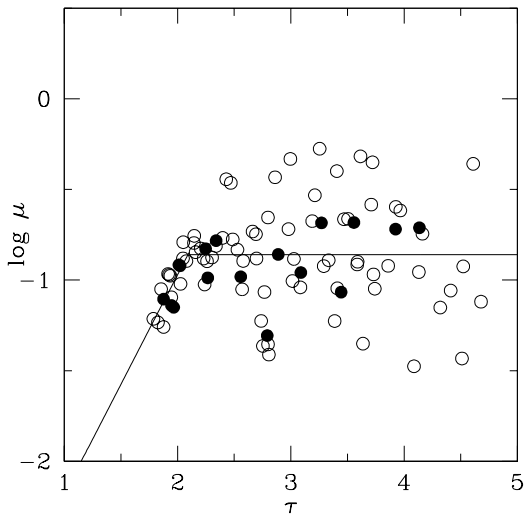


Fig. 3.— LMC (open symbols) and SMC (filled symbols) PN, all morphologies except bipolar PN are plotted. Solid line: our new calibration for the Magellanic Cloud PNe.

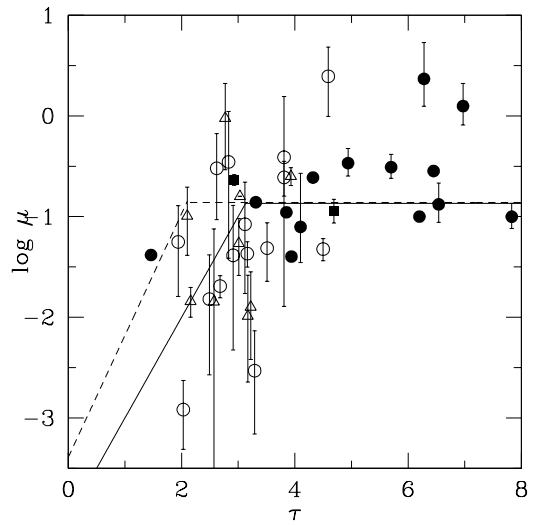


Fig. 4.— The Galactic PNe of known distances plotted on the $\tau - \log \mu$ plane. Lines as in Figure 3. Symbols denote the method used for individual distance determination. Filled circles: P; filled squares: CM; open circles: R; open triangles: E.

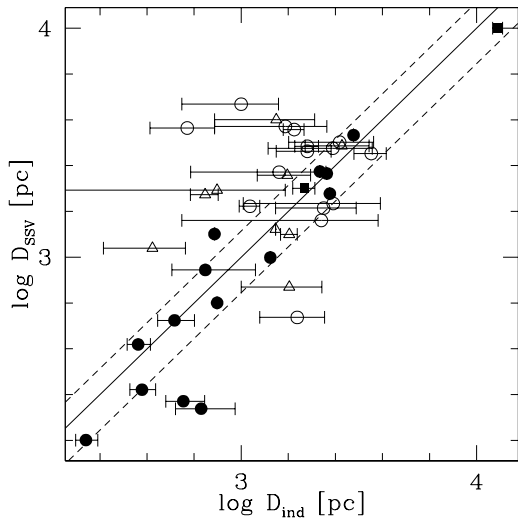


Fig. 5.— Comparison of statistical distances from our new calibration (SSV) with individual distances of Table 2. Symbols represent the individual distance determination method, as in Fig. 5. Solid line: 1:1. Broken lines represent the 30% differences between statistical and individual distances.

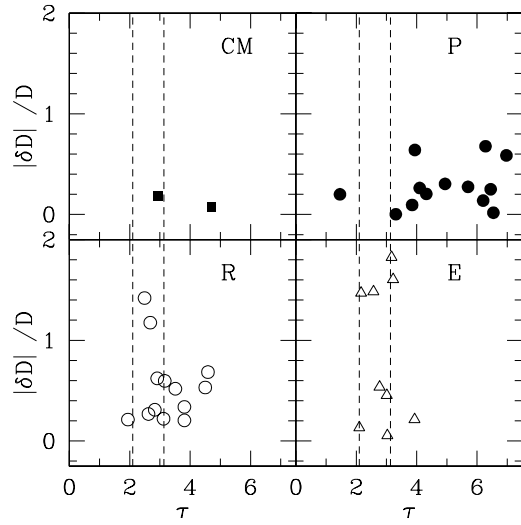


Fig. 6.— Relative differences between SSV statistical and individual PN distances, as a function of τ , separated in the panels by individual distance method. Symbols as in Fig. 6. Vertical lines denotes the τ of the thick to thin transition for the CKS and the SSV scales.

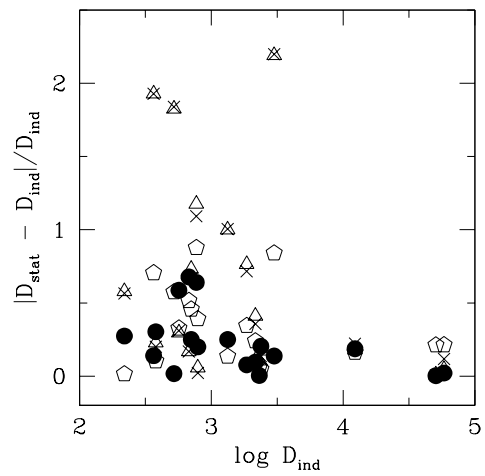


Fig. 7.— Relative differences between statistical and individual PN distances, plotted against the individual distances, for the Magellanic Cloud PN-calibrated scales of CKS (filled symbols), vdSZ (triangles), BL01 (crosses) and SB96 (pentagons).